Chemical Science

ROYAL SOCIETY OF CHEMISTRY

EDGE ARTICLE

View Article Online
View Journal | View Issue

Cite this: *Chem. Sci.*, 2022, **13**, 11174

All publication charges for this article have been paid for by the Royal Society of Chemistry

Received 6th June 2022
Accepted 28th August 2022

DOI: 10.1039/d2sc03167a

rsc.li/chemical-science

Size-dependent properties and unusual reactivity of novel nonplanar heterocycloarenes†

Jiangyu Zhu, Wenhao Li, Ning Zhang, Dongyue An, Yan Zhao, Xuefeng Lu * and Yunqi Liu *

The solution-phase synthesis of (hetero)cycloarenes with a well-defined size and geometric structure remains a challenging topic in organic chemistry and materials science. Herein, two novel nonplanar N,S-heterocycloarenes (**PTZ1** and **PTZ2**) containing two/three alternate phenothiazine-*co*-phenanthrene units were conveniently synthesized. The smaller size heterocycloarene **PTZ1** adopts a unique butterfly-shaped geometry and shows moderate supramolecular host–guest interactions with both fullerenes C_{60} and C_{70}; whereas the higher homologue **PTZ2** has a saddle-shaped conformation and demonstrates no obvious encapsulation with C_{60} or C_{70}. Meanwhile, benefiting from the relatively ordered molecular packing, the thin film of **PTZ1** behaved as a p-type semiconductor, while the more distorted **PTZ2** does not display any field-effect characteristics. Particularly, upon the oxidation of heterocycloarene **PTZ1** by Oxone, an unusual bis(sulfone-*co*-orthoquinone) product **PTZ1-Oxi** with an arc-shaped geometry is obtained and identified by single-crystal X-ray analysis. Our findings markedly expand the known chemistry of (hetero)cycloarenes and open a new path for their further functionalization.

Introduction

Cycloarenes are a unique class of fully annelated π-conjucated macrocycles with a fascinating electronic structure and diverse molecular geometry and have recently attracted increasing attention in both organic synthetic chemistry and materials science.[1] The first typical example of cycloarenes, kekulene (Fig. 1a), consisting of 12 circularly fused benzene rings with D_{6h} symmetry was successfully synthesized by Staab and Diederich in 1978.[2] Single-crystal X-ray analysis and ^{1}H NMR spectroscopy reveal that the π-electrons in kekulene are mainly localized on individual benzenoid rings rather than delocalized throughout the entire macrocyclic framework.[3] Kekulene is also the smallest macrocyclic nanographene; therefore, cycloarenes can be considered as model molecules of periodic "graphene meshes" to study and understand defects in graphene.[4] Over the next few decades, two effective strategies have been used to create molecular diversity and tune the properties of cycloarenes. The first approach is to enlarge or decrease the conjugated skeleton of kelulene.[4a,5] In 1986, a contracted kekulene molecule containing 10 fused benzene rings was successfully synthesized by Staab and Funhoff.[5a] And in 2012, a higher heptagonal homologue of kekulene, septulene, containing 14 fused benzene rings was developed by King's group.[5b] In 2016, a higher octagonal homologue of kekulene, octulene (Fig. 1a), containing 16 fused benzene rings was achieved by Stępień and co-workers and used to bind chloride anions.[4a] Last year, a series of aryl-substituted edge-extended kekulenes were reported by Wu's group.[5c] The other strategy is to integrate heteroatoms directly into cycloarenes that would lead to heterocycloarenes, which can be regarded as the isoelectronic species of their hydrocarbon cousins but display different molecular geometries, electronic structures, and materials properties.[6] In 2013, Stępień and Myśliwiec reported a nitrogen-containing heterocycloarene (Fig. 1a) by introducing carbozole units and is isoelectronic to kekulene and adopts a bowl-shaped conformation.[6a] In 2018, a saddle-shaped S-embedded heterocycloarene was synthesized by Miao's group and applied into thin-film field-effect transistors (FETs) and exhibited a hole mobility of 2.7×10^{-4} cm^2 V^{-1} s^{-1}.[6b] More recently, our group and co-workers also developed another saddle-shaped S-containing heterocycloarene S-octulene by replacing two benzene rings with two thiophene rings in octulene, which is the isoelectronic species of octulene and showed p-channel transport characteristics with a hole mobility of 1.1×10^{-3} cm^2 V^{-1} s^{-1} at room temperature.[6c] Moreover, a few open-shell cyclopenta-fused cycloarenes with fantastic (anti)aromaticity were reported.[7] However, despite their great potential applications in host–guest assemblies and organic optoelectronics, only a handful of (hetero)cycloarenes have been synthesized, and several of them have been documented as organic

Department of Materials Science, Fudan University, Shanghai 200433, China. E-mail: luxf@fudan.edu.cn; liuyq@fudan.edu.cn

† Electronic supplementary information (ESI) available: Synthetic procedures and characterization data of all physical characterization and theoretical calculations; and additional spectroscopic data. CCDC 2172358 and 2172326. For ESI and crystallographic data in CIF or other electronic format see https://doi.org/10.1039/d2sc03167a

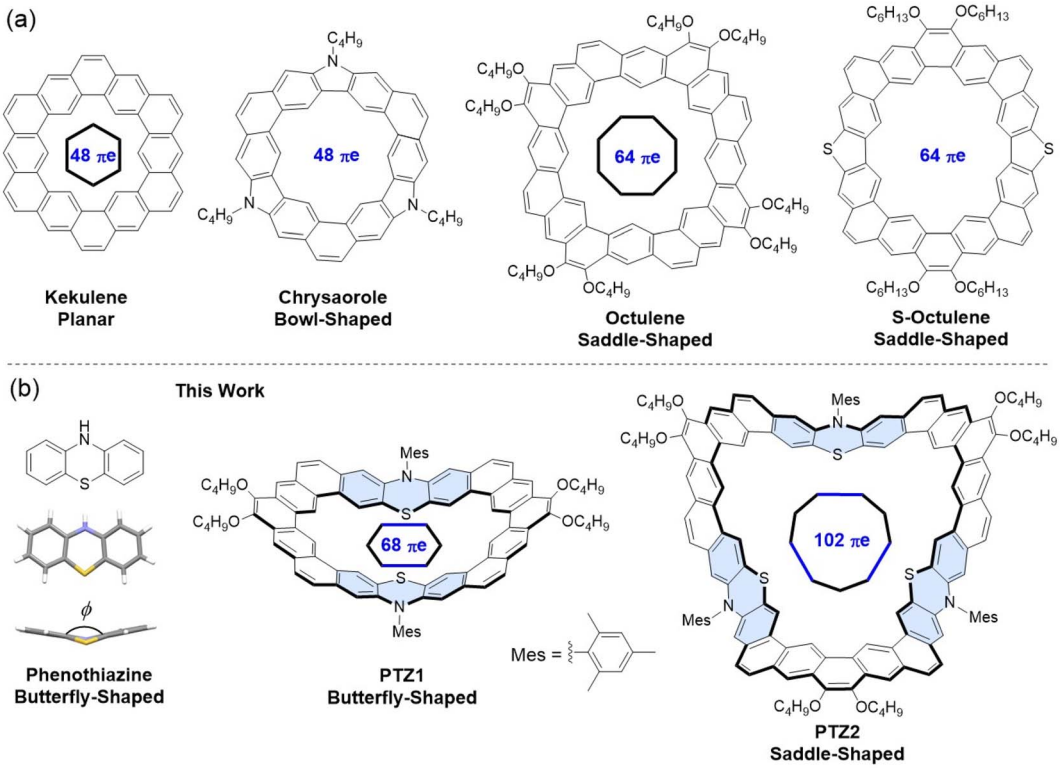

Fig. 1 (a) Chemical structures of some reported cycloarenes and heterocycloarenes constructed with planar building blocks. (b) Structures of new N,S-heterocycloarenes containing phenothiazine units.

semiconductors, because the size- and structure-selective synthesis of (hetero)cycloarenes remains a significant challenge.[1]

Recently, some nonplanar (hetero)cycloarenes have been constructed by using planar building blocks, such as carbazole, phenanthrene and dibenzothiophene, which may bring high strain during the subsequent cyclization process.[4a,6c] Herein, we are particularly interested in utilizing an intrinsic nonplanar building unit to construct less-strain curved heterocycloarenes. Phenothiazine is an important class of tricyclic electron-donor unit with a nonplanar butterfly structure (Fig. 1b)[8] and largely used as the active component in new push–pull chromophores for organic optoelectronic applications.[9] The incorporation of phenothiazine into cycloarene offers the unique properties associated with the 1,4-thiazine subunit, (i) the bent conformation may enable access to less strain, (ii) the electron-rich and intrinsic curved structure originating from S- and N-atoms may result in diverse supramolecular self-assembly behaviors,[10] and (iii) the sulfur atom can afford oxidation active sites to facilitate subsequent research on reactivity.[11] In this context, we report two novel fully fused N,S-heterocycloarene homologues (**PTZ1** and **PTZ2**, Fig. 1b), containing two and three alternately linked phenothiazine and alkoxyl-substituted phenanthrene subunits, respectively. According to X-ray single crystal analysis, host–guest NMR titrimetric experiments, and density functional theory (DFT) calculations, the smaller size heterocycloarene **PTZ1** has a unique butterfly-shaped conformation with 68 π-electrons, which can be regarded as an expanded hetero-kekulene with extension of two opposite edges and exhibits moderate supramolecular host–guest interactions with both fullerenes C_{60} and C_{70}, whereas the higher homologue **PTZ2** is a nonagonal heterocycloarene with 102 π-electrons and adopts a saddle-shaped geometry and demonstrates no obvious encapsulation with C_{60} or C_{70}. Meanwhile, benefiting from the relatively regular geometry and ordered molecular packing, organic thin-film field-effect transistor devices based on **PTZ1** display an improved hole mobility up to 0.002 $cm^2 V^{-1} s^{-1}$, while the more distorted heterocycloarene **PTZ2** does not show noticeable field-effect response. In addition, considering that the sulfur atom in phenothiazine is feasible to be oxidized into sulfoxide or sulfone, we are also interested in exploring the chemical reactivity of N,S-heterocycloarenes, which is beneficial to the structural diversity and functionalization of heterocycloarenes and has not been studied before in (hetero)cycloarenes. Particularly, upon the oxidation of heterocycloarene **PTZ1** by the convenient oxidant Oxone, an unexpected arc-shaped bis(sulfone-*co*-orthoquinone) product **PTZ1-Oxi** is obtained and verified by ^{1}H NMR spectroscopy and single-crystal X-ray analysis, suggesting that not only the sulfur atoms but also the adjacent alkoxy groups of the phenanthrene unit are oxidized. Our studies give some new insights on designing novel curved hetercycloarenes and pave an effective path to further functionalize the heterocycloarenes.

Results and discussion

Synthesis, geometry and aromaticity

The synthetic approach for the preparation of curved N,S-heterocycloarenes **PTZ1** and **PTZ2** is depicted in Scheme 1. The synthetic strategy is similar to our previous reports.[6c] Butoxy groups and bulky mesityl groups are used to ensure suitable solubility. By a Suzuki coupling reaction between equimolar amounts of **1** and **2** using XPhos Pd G2 as a catalyst, the dimeric macrocycle **3a** and trimeric macrocycle **3b** were synthesized and purified by recycling preparative gel permeation chromatography in 24% and 12% yields, respectively. Subsequently, **3a** and **3b** were converted to the corresponding tetramethoxyethenylated precursor **4a** and hexamethoxyethenylated precursor **4b** through the Wittig reaction. In the last step, treatment of **4a** and **4b** with $Bi(OTf)_3$ catalyzed intramolecular Friedel–Crafts alkylation gave the expected fully fused N,S-heterocycloarene **PTZ1** and **PTZ2**, respectively, which were isolated by normal silica gel column chromatography. Both **PTZ1** and **PTZ2** are yellow solids and can well dissolve in common organic solvents, such as dichloromethane, chloroform, toluene, and THF. All new products were characterized by $^1H/^{13}C$ NMR and high-resolution mass spectroscopy. The aromatic atoms of **PTZ1** and **PTZ2** were further assigned using the 2D NOESY NMR spectra (Fig. S1 and S2†). The low-field resonance of inner protons indicates that π-electrons are localized into individual rings, rather than globally delocalized over the entire macrocyclic backbone, which is similar to septulene and octulene.[4a,5b]

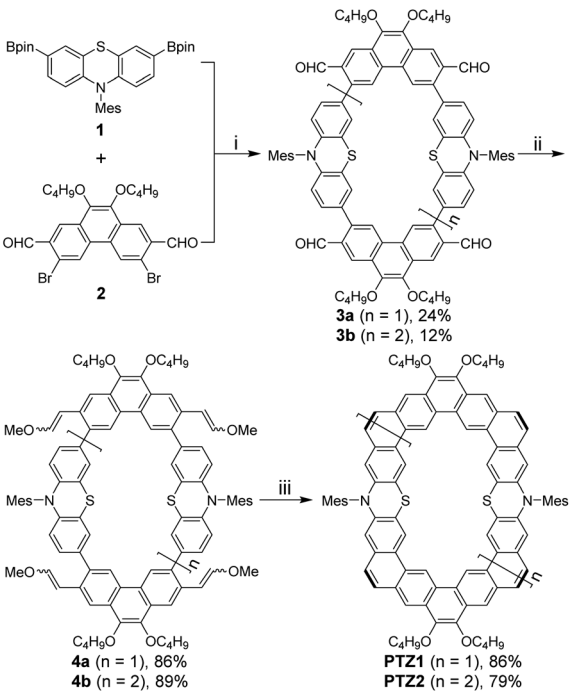

Scheme 1 Synthetic route for heterocycloarenes PTZ1 and PTZ2: (i) XPhos Pd G2, K_3PO_4, THF/H_2O, and 55 °C; (ii) (methoxymethyl)triphenylphosphonium chloride, *t*-BuOK, and THF; (iii) $Bi(OTf)_3$ and dichloroethane.

Single crystals of **PTZ1** were successfully grown by slow diffusion of acetonitrile into the chloroform solution, and its X-ray crystallographic structure is shown in Fig. 2, which clearly reveals a butterfly-shaped geometry. There is a defined cavity in **PTZ1** with a large diameter of 11.80 Å and a small diameter of 5.80 Å. The dihedral angle of the butterfly-shaped structure is 140.74°. The neighbouring molecules in the single-crystal of **PTZ1** arrange in opposite direction with a molecular spacing of 9.45 Å and adopt a one-dimensional (1D) slipped column stacking (Fig. 2b). The interplanar distances of the adjacent molecules between the planes defined by half of the π systems were measured to be 3.39 Å for concave pairs and 3.56 Å for convex pairs. The close molecule packing is beneficial to intermolecular charge transport, indicating the potential application in OFET.[12] Adjacent columns, with a different angle of inclination, are further packed independently into a three-dimensional (3D) structure without any interaction. Unfortunately, the single-crystal structure of **PTZ2** could not be obtained despite much effort, thus its geometry was optimized by DFT calculations at the B3LYP/6-31G(d,p) level of theory,[13] replacing butoxy groups by methoxy groups for simplification (Fig. 2c). **PTZ2** shows a very deep saddle-shaped conformation with the depth of 8.89 Å and a larger cavity with the smallest diameter of about 8.28 Å. The enormous difference in geometry between **PTZ1** and **PTZ2** may be attributed to the distortion formed by the larger-size macrocycle.

To further understand the aromaticity of the N,S-heterocycloarenes, bond-length analysis, nucleus independent chemical shift (NICS)[14] and anisotropy of the induced current density (ACID)[15] were carried out. As shown in Fig. 2a, the bond *a* (1.337 Å) in the middle six-membered ring of the phenanthrene unit and the bond *b* (1.349 Å) formed by the Friedel–Crafts reaction are obviously shorter than that of the typical $C(sp^2)$–$C(sp^2)$ double bond (1.39 Å) in benzene[16] and close to that of in a typical olefin (1.33–1.35 Å),[16] which suggests that the bonds *a* and *b* prefer to act as a double bond. The $NICS(1)_{zz}$ values (−9.0 ppm and −14.3 ppm) of corresponding six-membered rings reveal less aromatic character of rings E and C, compared to −29.3 ppm of benzene,[17] which is common in other (hetero)cycloarenes.[5c,6c] In addition, it should be noted that the $NICS(1)_{zz}$ value for the thiazine ring A is +6.3 ppm, indicating that its antiaromaticity because of the existing N and S atoms results in a six-membered thiazine heterocycle with 8 ([4*n*]) conjugated π electrons. By analyzing the aromaticity of large macrocycle **PTZ2** (Fig. 2d), we can obtain a similar conclusion. The ACID plots of the macrocycles **PTZ1** and **PTZ2** display two and three local clockwise ring current flows including six fused rings separated by thiazine rings (Fig. 8a and S14†), respectively, implying the local aromaticity. All the above analysis results suggest the local aromaticity in phenothiazine-containing N,S-heterocycloarenes, which further verifies the Clar's picture of local aromatic sextets.[3b]

Optical and electrochemical properties

The photophysical properties of N,S-heterocycloarenes in toluene were investigated by UV-vis absorption and

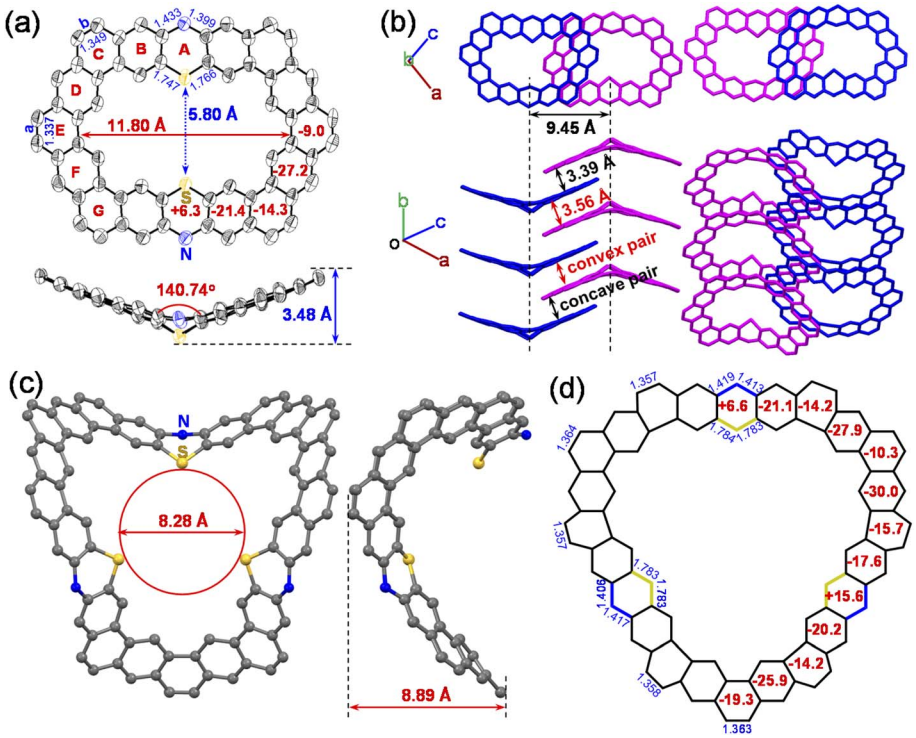

Fig. 2 (a) X-ray crystallographic structure and selected bond lengths (in Å) of **PTZ1** (b) crystal packing in the top view and side view of **PTZ1**. (c) Optimized (B3LYP/6-31G(d,p)) structure of **PTZ2**. (d) Selected bond lengths (in Å) of **PTZ2**. The red numbers in the individual rings (a)/(d) are calculated NICS(1)$_{zz}$ values (ppm). Hydrogen atoms and aryl/alkoxy substituents are omitted for clarity.

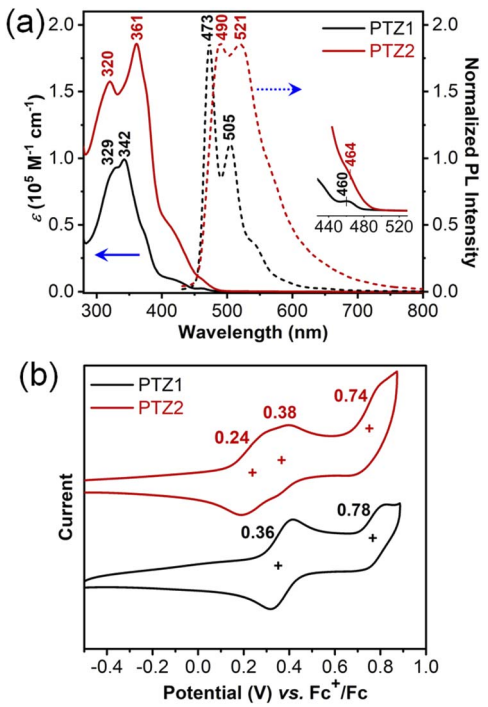

Fig. 3 (a) UV-vis absorption and normalized fluorescence spectra of **PTZ1** and **PTZ2** measured in toluene, and the inset is the magnified onset absorption band. (b) Cyclic voltammogram of **PTZ1** and **PTZ2** dissolved in dichloromethane.

fluorescence spectroscopies (Fig. 3a). The molar absorption coefficients of **PTZ1** and **PTZ2** were measured to be 0.99 × 10^5 M^{-1} cm^{-1} and 1.86 × 10^5 M^{-1} cm^{-1}, respectively. The weak shoulder peaks at 460 nm for **PTZ1** and 464 nm for **PTZ2** were observed, which can be correlated to the HOMO → LUMO transition with small oscillator strength according to the time-dependent (TD) DFT calculations (Table S4 and S5†).[18] In addition, the maximum absorption wavelength of **PTZ2** (λ_{max} = 361 nm) is longer compared with that of compound **PTZ1** (λ_{max} = 342 nm), which can be explained by the extended π-conjugation system. However, the red-shift turns very minor at the absorption onsets, which could be due to the cooperation between the extended conjugation and distorted structure, as observed in other big-size macrocycles.[10c] The optical energy gap (E_g^{opt}) was estimated to be 2.60 eV and 2.57 eV for **PTZ1** and **PTZ2**, respectively. Moreover, the bathochromic shift in the fluorescence spectra between **PTZ1** and **PTZ2** is 17 nm, which is similar to the corresponding absorption spectra. The fluorescence quantum yields of **PTZ1**and **PTZ2** in the 0.1 mol L^{-1} H_2SO_4-toluene system, with the quinine sulfate as the standard, were determined to be 2.7% and 2.3%, respectively.

Cyclic voltammetry (CV) and differential pulse voltammetry (DPV) measurements of **PTZ1** and **PTZ2** were performed in dry DCM by using 0.1 M tetra-*n*-butylammonium hexfluorophosphate as the electrolyte (Fig. 3b and S3†). **PTZ1** displayed two reversible oxidation waves with a half-wave potential ($E_{1/2}^{ox}$) at 0.36 and 0.78 V (*vs.* Fc^+/Fc); **PTZ2** exhibited three quasi-reversible oxidation waves with a $E_{1/2}^{red}$ at 0.24, 0.38 and

0.74 V. According to the NMR spectroscopic and X-ray analyses, **PTZ1** and **PTZ2** have high symmetry with identical phenothiazinyl moieties, so the separated oxidation behavior of the N,S-heterocycloarene may be due to the intramolecular electronic communication, which is observed for phenothiazine-containing cyclophanes.[19] DFT calculations were performed at the B3LYP/6-31G(d,p) level to investigate the electronic properties of the phenothiazine-containing N,S-heterocycloarenes by using the simplified model molecules. As shown in the Fig. S13†, the HOMO of **PTZ1** delocalizes over the whole aromatic backbone, while the LUMO essentially localizes on the phenanthrene units. The delocalized distribution of the HOMO is in agreement with the considerable conjugation between the phenanthrene and phenothiazine units in **PTZ1**. With the appropriate electronic energy level and the delocalized HOMO, **PTZ1** is a potential p-type semiconductor material.[20] However, the HOMO of the large-size heterocycloarene **PTZ2** distributes unevenly, on account of the deeply distorted skeleton structure, and the LUMO localizes on the one of the three phenanthrene units, which also indicates the low conjugation extent among moieties of **PTZ2** (Fig. S14†).

Semiconductor properties

The charge carrier transport was studied in thin-film OFETs based on a bottom-gate bottom-contact (BGBC, Fig. 4a) configuration. The 300 nm SiO_2 surface dielectric layer was functionalized with octadecyltrichlorosilane (OTS) to minimize interfacial trapping sites. The heterocycloarene thin films were deposited by spin-coating 6 mg mL^{-1} $CHCl_3$ solution with a speed of 3000 rpm for 60 seconds in a nitrogen atmosphere. OFET devices were measured in a glovebox with a Keysight 4200. Obvious difference in transistor performance was observed between **PTZ1** and **PTZ2**. While the larger size heterocycloarene **PTZ2** did not exhibit any field-effect response, maybe due to the more distorted molecular structure, the smaller size heterocycloarene **PTZ1** with relatively regular geometry and ordered molecular packing functioned as a p-type semiconductor and showed a hole mobility of 2.1×10^{-3} cm^2 V^{-1} s^{-1}; the corresponding transfer and output characteristic curves are presented in Fig. 4; meanwhile, the film morphology and microstructure of the spin-cast film were examined *via* atomic force microscopy (AFM) and thin-film XRD. The film surface of **PTZ1** displayed smooth morphology with low surface roughness (root-mean square RMS = 0.31 nm), which is beneficial to charge injection. However, as shown in Fig. S11†, there wre no diffraction peaks in the XRD pattern, which represents the low crystallinity of the film. Therefore, the low mobility may have originated from the intrinsic nonplanar butterfly-shaped backbone of the material and the poor molecular alignment of the thin film, which limits the intramolecular and intermolecular charge transport.

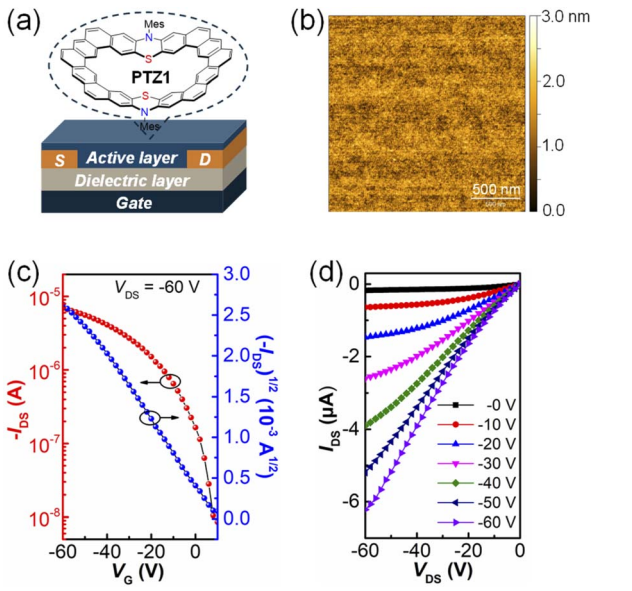

Fig. 4 (a) BGBC device structure. (b) AFM images of the PTZ1 thin film with small grain size. (c) Transfer and (d) output characteristics of OFET devices based on PTZ1.

Host–guest interaction with fullerenes

It's well known that (hetero)cycloarenes with a unique topological and electronic structure are capable of binding with ions[4a] and small molecules,[6c] so we studied the host–guest supramolecular chemistry of **PTZ1** and **PTZ2**. Considering that **PTZ1** and **PTZ2** are electron-rich and have defined cavities, we chose fullerenes C_{60} and C_{70} as the receptor. The ^{1}H NMR titration experiments in tolulene-d_8 were carried out to monitor the binding behavior at 298 K (Fig. S4–S7†). With the increasing concentration of fullerenes, all the protons on the skeleton of **PTZ1**, especially the inner ring protons ($H_{a,\ b}$), are shifted to high field. When 0.5 equivalent of C_{60} or C_{70} was added into **PTZ1**, the upfield shifts tended to saturate ($\Delta\delta = 0.03/0.06$ ppm), indicating the establishment of π interactions between them and formation of the 2 : 1 host/guest stoichiometric binding (Fig. 5a). By fitting the ^{1}H NMR data with the 2 : 1 binding mode, the binding constants K_{11}/K_{21} of **PTZ1** were calculated to be 1.2 M^{-1}/6.7 $\times$ 10^6 M^{-1} for C_{60} and 17.3 M^{-1}/9.3 $\times$ 10^5 M^{-1} for C_{70} (Fig. S8†).[21] As we fitted as described above, K_{11} is negligible in comparison to K_{21}, indicating positive cooperative complexation of fullerenes with **PTZ1**. This could be the reason that the fullerenes are sandwiched between two N,S-heterocycloarenes, which has been reported for many other macrocycles.[22] In addition, the C_{70} toward **PTZ1** ($K_a = 16.1 \times 10^6$ M^{-2}) has about twice the binding affinity of C_{60} ($K_a = 8.3 \times 10^6$ M^{-2}), which shows that the C_{70} with larger ellipsoidal geometry is more complementary with the butterfly-shaped aromatic surface of **PTZ1** than C_{60} (Table S2†). Meanwhile, the stronger binding affinity of **PTZ1** toward C_{70} was also verified by fluorescence titration experiments. (Fig. S9 and S10†) However, when the same equivalent (0.5 equiv.) or even up to 2 equiv. of C_{60} or C_{70} was added into **PTZ2**, the ^{1}H signal of **PTZ2** remains essentially unaltered (Fig. 5b and Fig. S6 and S7†). It indicates no obvious binding between **PTZ2** and fullerene (C_{60} or C_{70}), which may because the fullerenes do not match with both the cavity size and geometric shape of **PTZ2**.[23]

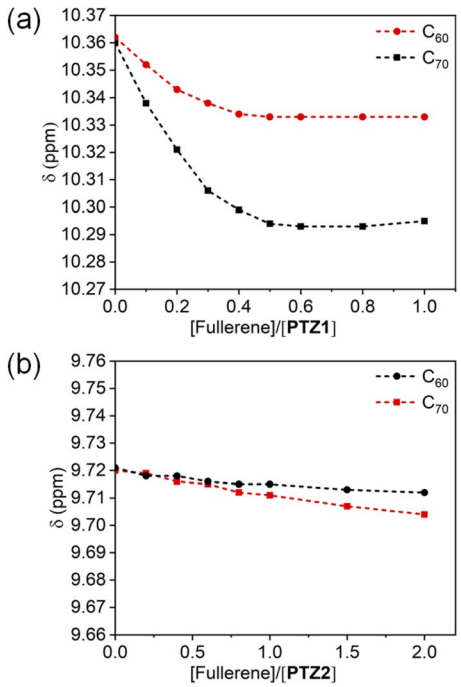

Fig. 5 Changes of chemical shift of proton H_a for ^{1}H NMR (400 MHz, CD_2Cl_2) titration for **PTZ1** (a) and **PTZ2** (b) with C_{60} and C_{70}.

Oxidation of N,S-heterocycloarene

Since the sulfur in phenothiazine can be easily oxidized into sulfoxide and further to sulfone, we plan to oxidize **PTZ1** as a model of N,S-heterocycloarenes to explore its reactivity. Therefore, we oxidized **PTZ1** with excess Oxone and $NaHCO_3$ in a mixed solvent system of acetone/CH_2Cl_2/H_2O (1 : 1 : 1, v/v/v) at room temperature overnight (Fig. 6a). After simple purification by gel column chromatography, the crude product through recrystallization led to few of orange crystals from a mixed solution of CH_3Cl/CH_3OH. The ^{1}H NMR spectrum of the oxidized product is shown in Fig. 6b, and it is noted that there are seven aromatic signals reflecting the highest possible C_{2v} symmetry. Interestingly, there are no signals in the range of 3.5–5.0 ppm in the ^{1}H NMR spectra, which reveals that the alkoxy groups on phenanthrenes of **PTZ1** were oxidized. Meanwhile, MALDI-TOF MS demonstrates that the resulting product lost four alkoxy groups and contains eight additional oxygen atoms as compared with **PTZ1** (Fig. S39†). The structure of this product was finally confirmed by single crystal X-ray structure analysis (Fig. 7). The single crystal of **PTZ1-Oxi** was grown by slow diffusion of methanol into a $CHCl_3$ solution at room temperature. The bond length linked oxygen atoms to phenanthrene units were 1.212 Å and 1.210 Å, which are close to that of the typical ketone,[24] all suggesting that not only the sulfur atoms but also the alkoxy groups of **PTZ1** were oxidized to give the bis(sulfone-*co*-orthoquinone) product **PTZ1-Oxi**. In general, the oxidation of an aromatic ring needs harsh reaction conditions. The easy oxidation of phenanthrene in **PTZ1** is attributed to its less aromatic character, so that the bond linked two alkoxy

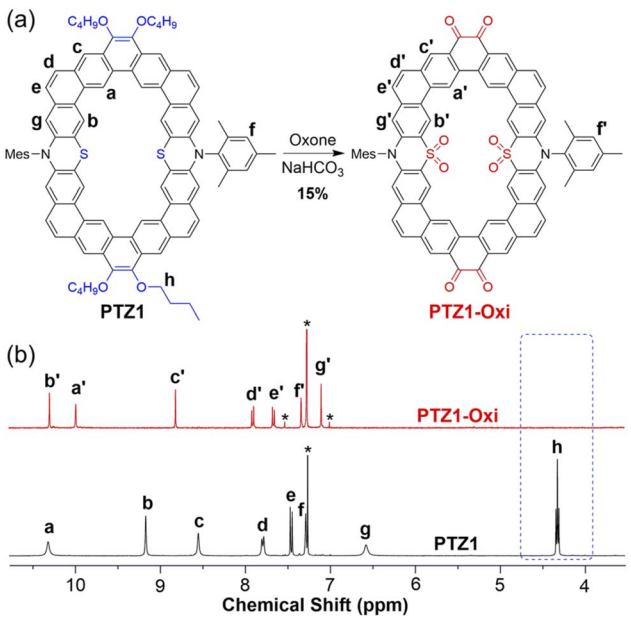

Fig. 6 (a) Oxidation of the N,S-heterocycloarene **PTZ1**. (b) Partial ^{1}H NMR spectra of **PTZ1** and its oxidation product **PTZ1-Oxi** in $CDCl_3$. The peaks labeled by an asterisk indicate residue solvents and satellite peaks.

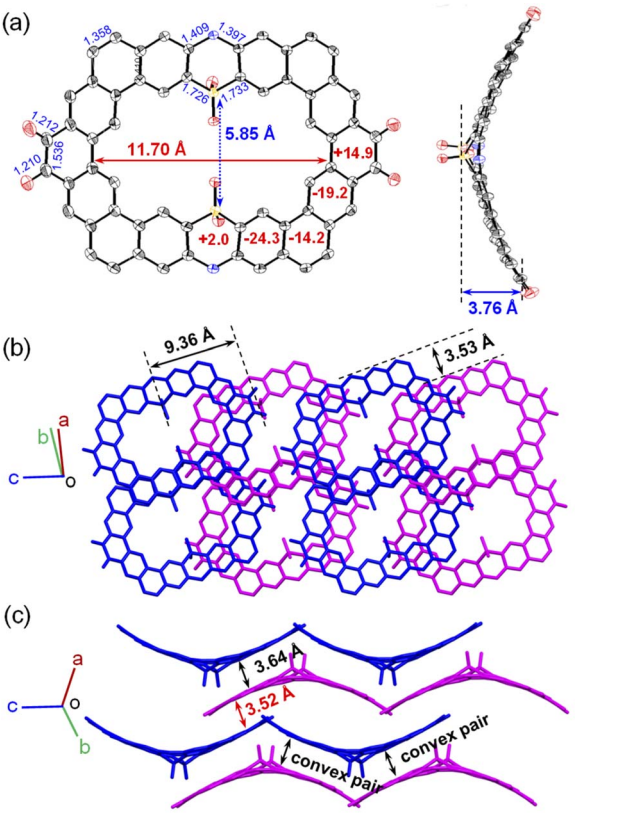

Fig. 7 (a) Crystal structure and selected bond lengths (in Å) of **PTZ1-Oxi**. The red numbers in the individual rings are calculated NICS(1)$_{zz}$ values (ppm). Crystal packing viewed along the top view (b) and the side view (c).

prefers to behave as an olefin. Unfortunately, it is difficult to obtain ^{13}C NMR and 2D NOESY NMR spectra of oxidized product **PTZ1-Oxi** due to the low solubility. So we calculated the chemical shift of **PTZ1-Oxi** to distribute the aromatic proton at the B97-2/pcSseg-1 level of theory (Table S7†).[25] The upfield of the proton H_a indicates that the proton H_a is positioned in the shielding region after oxidation. The rest of the aromatic protons are shifted to low field because of the electron-withdrawing effect from the sulfone.

From the single crystal analysis (Fig. 7), we noticed that the crystal alignment changed from a monoclinic system for **PTZ1** to a triclinic system for **PTZ1-Oxi**. The **PTZ1-Oxi** adopts an arc-shaped geometry instead of a butterfly structure; meanwhile, the depth of the arc is slightly increased to 3.76 Å (Fig. 7a). The arc molecules in the single crystal form convex pairs with surrounding two molecules by the π-orbital overlap with an interplanar distance of 3.64 Å and arrange in a layer (Fig. 7c). Meanwhile, the overlap of the convex pair in **PTZ1-Oxi** concentrates the benzo[*m*]tetraphene moiety instead of the pentaphene moiety in **PTZ1** (Fig. 7b), which could be attributed to the donor-acceptor (D-A) interaction between dioxophenothiazine and phenanthrenequinone. Moreover, there is a small π-orbital overlap between the molecules in adjacent layers with an interplanar distance of 3.52 Å. All the above suggest that the crystal of **PTZ1-Oxi** adopts a tighter 2D slipped stacking mode rather than the 1D slipped stacking structure for **PTZ1**, which can be ascribed to the D–A molecular structure and the absence of constraints from alkoxy substituents.

Furthermore, as shown in Fig. 7a, the length of the bond linking two carbonyl groups in the phenanthrene unit is 1.536 Å, which is the typical bond length of $C(sp^3)$–$C(sp^3)$ (1.53–1.55 Å).[25] Incorporation of $C(sp^3)$ indicates that the conjugation of the macrocycle is broken. Meanwhile, the changes of the bond may significantly affect the aromaticity of the phenothiazine-containing heterocycloarenes. The $NICS(1)_{zz}$ values of the ring E changes from −9.0 for **PTZ1** to +14.9 for **PTZ1-Oxi**, demonstrating the transition from weak aromaticity to antiaromaticity (Fig. 7a). With the loss of two π-electrons on the sulfur atom, the calculated $NICS(1)_{zz}$ value of ring A changes from +6.3 to +2.0, indicating the reduced antiaromaticity. Moreover, other rings on the skeleton have changed in varying degrees, which suggests that the oxidation has strong influence on the aromaticity of surrounded aromatic rings. The ACID plot of **PTZ1-Oxi** is shown in Fig. 8b. Compared with **PTZ1**, each current flow including six fused rings is broken into two current flows including three fused rings by the carbonyl groups. These current flows all display a local clockwise characteristic, indicating the local aromaticity.

The optical properties of **PTZ1-Oxi** were characterized from the UV-vis absorption and fluorescence spectra (Fig. S12†). The absorption onset of **PTZ1-Oxi** exhibited a bathochromic shift of 67 nm compared with unoxidized product **PTZ1** and resulted in more narrow energy gap of 2.28 eV (Table S1†), which is consistent with the TD-DFT calculations (Fig. S15†). The bathochromic shift effect indicates the formation of efficient intramolecular charge transfer (ICT) in the oxidized product **PTZ1-Oxi**, which is common in some D–A molecules.[26] The red-shift is also observed in the fluorescence spectra (Fig. S12a†). The CV spectrum of **PTZ1-Oxi** displays two quasi-reversible oxidation waves with a $E_{1/2}^{ox}$ at 0.78 and 0.99 eV for the two dioxophenothiazine units and one quasi-reversible reduction wave with a $E_{1/2}^{ox}$ at −1.37 eV probably for the phenanthrenequinone moiety. The HOMO/LUMO energy level of **PTZ1-Oxi**, which was estimated to be −5.49/−3.21 eV, is lower than that of **PTZ1** (−5.09/−2.49 eV). The decreased energy level can be attributed to the loss electrons of sulfur atoms and incorporation of carbonyl groups by oxidation. Moreover, the HOMO of **PTZ1-Oxi** delocalizes over the whole skeleton similar to that of **PTZ1** (Fig. 8c). However, the LUMO mainly localizes at the C=O bonds of the phenanthrenequinone units, attributing to the electron-withdrawing effect of the carbonyl groups.

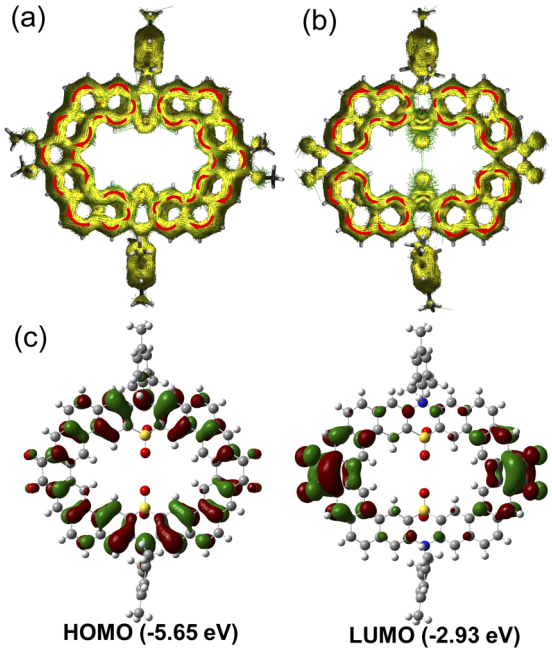

Fig. 8 Calculated ACID plots (contribution from π electrons only) of (a) PTZ1 and (b) PTZ1-Oxi with isovalues of 0.019 and 0.030, respectively. The magnetic field is perpendicular to the *XY* plane and points out through the paper. (c) Calculated frontier orbitals and energy levels of PTZ1-Oxi.

Conclusions

In summary, we successfully synthesized two fully annelated nonplanar N,S-heterocycloarenes with different sizes (**PTZ1** and **PTZ2**) by a macrocyclization followed by a periphery fusion strategy using curved building blocks. X-ray single crystal analysis, DFT calculations and NMR titrimetric experiments reveal that the small-size heterocycloarene **PTZ1** has a butterfly-shape conformation and can form supramolecular complexes with both fullerenes C_{60} and C_{70}, while the large-size heterocycloarene **PTZ2** adopts a saddle-shaped geometry without obvious encapsulations with C_{60} or C_{70}. Meanwhile, benefiting from regular geometry, ordered π–π stacking and a suitable electronic energy level, the BGBC organic field effect transistor

devices based on **PTZ1** exhibited p-type charge transport with a hole mobility of 0.002 $cm^2 V^{-1} s^{-1}$, whereas no field effect mobility was observed for the more distorted heterocycloarene **PTZ2**. In addition, the clear size and geometry dependence of photophysical and electrochemical properties and aromaticity can be seen for this unique heterocycloarene system. Moreover, upon the oxidation of heterocycloarene **PTZ1** by Oxone, an unexpected arc-shaped bis(sulfone-*co*-orthoquinone) product **PTZ1-Oxi** is obtained and identified by ^{1}H NMR spectroscopy and X-ray crystallographic analysis, indicating that both the sulfur atoms and the adjacent alkoxy groups of the phenanthrene unit are oxidized. Interestingly, the oxidation has significant influences on the electronic structure, aromaticity, molecular stacking, and ICT interactions. Our work provides a general strategy for designing novel curved heterocycloarenes and paves a new path for further modification and post-functionalization of heterocycloarenes.

Data availability

The crystallographic data was provided in Cambridge Structural Database, and the other necessary data of this study have been provided in the ESI.†

Author contributions

X. L. and Y. L. supervised the project. X. L. and J. Z. designed the experiments, analyzed the data and co-wrote the manuscript. J. Z. performed all the synthetic experiments and characterization and theoretical calculations. W. L. assisted in OFET fabrication and characterization. N. Z. and D. A. assisted in the synthesis of compounds. Y. L., X. L., Y. Z. and J. Z. discussed the results and commented on the manuscript.

Conflicts of interest

There are no conflicts to declare.

Acknowledgements

This work was financially supported by the National Natural Science Foundation of China (52073063, 51903052, 51903051, and 61890940), the National Key R&D Program of China (2018YFA0703200), the Natural Science Foundation of Shanghai (22ZR1405800), and the Program for Professor of Special Appointment (Eastern Scholar) at the Shanghai Institutions of Higher Learning.

Notes and references

1 (*a*) J. C. Buttrick and B. T. King, *Chem. Soc. Rev.*, 2017, **46**, 7–20; (*b*) A. Borissov, Y. K. Maurya, L. Moshniaha, W. Wong, M. Żyła-Karwowska and M. Stępień, *Chem. Rev.*, 2022, **122**, 565–788; (*c*) M. Stępień, E. Gońka, M. Żyła and N. Sprutta, *Chem. Rev.*, 2017, **117**, 3479–3716.

2 F. Diederich and H. A. Staab, *Angew. Chem., Int. Ed. Engl.*, 1978, **17**, 372–374.

3 (*a*) R. McWeeny, *Proc. Phys. Soc., London, Sect. A*, 1951, **64**, 921–930; (*b*) E. Clar, *The Aromatic Sextet*, J. Wiley, New York, 1972.

4 (*a*) M. A. Majewski, Y. Hong, T. Lis, J. Gregoliński, P. J. Chmielewski, J. Cybińska, D. Kim and M. Stępień, *Angew. Chem., Int. Ed.*, 2016, **55**, 14072–14076; (*b*) A. W. Robertson, G.-D. Lee, K. He, C. Gong, Q. Chen, E. Yoon, A. I. Kirkland and J. H. Warner, *ACS Nano*, 2015, **9**, 11599–11607.

5 (*a*) D. J. H. Funhoff and H. A. Staab, *Angew. Chem., Int. Ed. Engl.*, 1986, **25**, 742–744; (*b*) B. Kumar, R. L. Viboh, M. C. Bonifacio, W. B. Thompson, J. C. Buttrick, B. C. Westlake, M. Kim, R. W. Zoellner, S. A. Varganov, P. Mörschel, J. Teteruk, M. U. Schmidt and B. T. King, *Angew. Chem., Int. Ed.*, 2012, **51**, 12795–12800; (*c*) W. Fan, Y. Han, X. Wang, X. Hou and J. Wu, *J. Am. Chem. Soc.*, 2021, **143**, 13908–13916; (*d*) W. Fan, Y. Han, S. Dong, G. Li, X. Lu and J. Wu, *CCS Chem.*, 2021, **3**, 1445–1452.

6 (*a*) D. Myśliwiec and M. Stępień, *Angew. Chem., Int. Ed.*, 2013, **52**, 1713–1717; (*b*) Y. Yang, M. Chu and Q. Miao, *Org. Lett.*, 2018, **20**, 4259–4262; (*c*) L. Yang, N. Zhang, Y. Han, Y. Zou, Y. Qiao, D. Chang, Y. Zhao, X. Lu, J. Wu and Y. Liu, *Chem. Commun.*, 2020, **56**, 9990–9993; (*d*) A. Tatibouët, R. Hancock, M. Demeunynck and J. Lhomme, *Angew. Chem., Int. Ed. Engl.*, 1997, **36**, 1190–1191; (*e*) M. Zhao, S. H. Pun, Q. Gong and Q. Miao, *Angew. Chem., Int. Ed.*, 2021, **60**, 24124–24130.

7 (*a*) S. Das, T. S. Herng, J. L. Zafra, P. M. Burrezo, M. Kitano, M. Ishida, T. Y. Gopalakrishna, P. Hu, A. Osuka, J. Casado, J. Ding, D. Casanova and J. Wu, *J. Am. Chem. Soc.*, 2016, **138**, 7782–7790; (*b*) H. Gregolińska, M. Majewski, P. J. Chmielewski, J. Gregoliński, A. Chien, J. Zhou, Y.-L. Wu, Y. J. Bae, M. R. Wasielewski, P. M. Zimmerman and M. Stępień, *J. Am. Chem. Soc.*, 2018, **140**, 14474–14480; (*c*) B. Prajapati, D.-K. Dang, P. J. Chmielewski, M. A. Majewski, T. Lis, C. J. Gómez-García, P. M. Zimmerman and M. Stępień, *Angew. Chem., Int. Ed.*, 2021, **60**, 22496–22504; (*d*) X. Lu, T. Y. Gopalakrishna, H. Phan, T. S. Herng, Q. Jiang, C. Liu, G. Li, J. Ding and J. Wu, *Angew. Chem., Int. Ed.*, 2018, **57**, 13052–13056; (*e*) X. Lu, T. Y. Gopalakrishna, Y. Han, Y. Ni, Y. Zou and J. Wu, *J. Am. Chem. Soc.*, 2019, **141**, 5934–5941; (*f*) X. Lu, D. An, Y. Han, Y. Zou, Y. Qiao, N. Zhang, D. Chang, J. Wu and Y. Liu, *Chem. Sci.*, 2021, **12**, 3952–3957.

8 (*a*) M. Sailer, M. Nonnenmacher, T. Oeser and T. J. J. Müller, *Eur. J. Org. Chem.*, 2006, **2006**, 423–435; (*b*) S. P. Massie, *Chem. Rev.*, 1954, **54**, 797–833; (*c*) F. R. Fronczek, *Cambridge Structural Database*, 2019, DOI: **10.5517/ccdc.csd.cc230v55**.

9 (*a*) I. J. Al-Busaidi, A. Haque, N. K. Al Rasbi and M. S. Khan, *Synth. Met.*, 2019, **257**, 116189; (*b*) J. Yang, M. Fang and Z. Li, *Aggregate*, 2020, **1**, 6–18; (*c*) J. Heo, D. P. Murale, H. Y. Yoon, V. Arun, S. Choi, E. Kim, J. Lee and S. Kim, *Aggregate*, 2022, **3**, e159; (*d*) Y. Im, M. Kim, Y. J. Cho, J.-A. Seo, K. S. Yook and J. Y. Lee, *Chem. Mater.*, 2017, **29**, 1946–1963.

10 (*a*) J. Wang, Y. Ju, K. Low, Y. Tan and J. Liu, *Angew. Chem., Int. Ed.*, 2021, **60**, 11814–11818; (*b*) H. Gregolińska, M. Majewski,

P. J. Chmielewski, J. Gregoliński, A. Chien, J. Zhou, Y. Wu, Y. J. Bae, M. R. Wasielewski, P. M. Zimmerman and M. Stępień, *J. Am. Chem. Soc.*, 2018, **140**, 14474–14480; (*c*) X. Lu, T. Y. Gopalakrishna, Y. Han, Y. Ni, Y. Zou and J. Wu, *J. Am. Chem. Soc.*, 2019, **141**, 5934–5941; (*d*) T. Iwamoto, Y. Watanabe, T. Sadahiro, T. Haino and S. Yamago, *Angew. Chem., Int. Ed.*, 2011, **50**, 8342–8344; (*e*) E. M. Pérez and N. Martín, *Chem. Soc. Rev.*, 2008, **37**, 1512–1519.

11 Y. Rout, C. Montanari, E. Pasciucco, R. Misra and B. Carlotti, *J. Am. Chem. Soc.*, 2021, **143**, 9933–9943.

12 C. Wang, H. Dong, W. Hu, Y. Liu and D. Zhu, *Chem. Rev.*, 2012, **112**, 2208–2267.

13 (*a*) A. D. Becke, *J. Chem. Phys.*, 1993, **98**, 5648–5652; (*b*) C. Lee, W. Yang and R. G. Parr, *Phys. Rev. B: Condens. Matter*, 1988, **37**, 785–789; (*c*) T. Yanai, D. P. Tew and N. C. Handy, *Chem. Phys. Lett.*, 2004, **393**, 51–57; (*d*) R. Ditchfield, W. J. Hehre and J. A. Pople, *J. Chem. Phys.*, 1971, **54**, 724–728; (*e*) W. J. Hehre, R. Ditchfield and J. A. Pople, *J. Chem. Phys.*, 1972, **56**, 2257–2261; (*f*) P. C. Hariharan and J. A. Pople, *Theor. Chim. Acta*, 1973, **28**, 213–222.

14 (*a*) Z. Chen, C. S. Wannere, C. Corminboeuf, R. Puchta and P. v. R. Schleyer, *Chem. Rev.*, 2005, **105**, 3842–3888; (*b*) P. v. R. Schleyer, C. Maerker, A. Dransfeld, H. Jiao and N. J. R. van Eikema Hommes, *J. Am. Chem. Soc.*, 1996, **118**, 6317–6318.

15 D. Geuenich, K. Hess, F. Köhler and R. Herges, *Chem. Rev.*, 2005, **105**, 3758–3772.

16 Anon, *Structure and Stability of Benzene*, **https://chem.libretexts.org/@go/page/31563**, (accessed 2022-5-10).

17 F. Alvarez-Ramírez and Y. Ruiz-Morales, *J. Chem. Inf. Model.*, 2020, **60**, 611–620.

18 N. M. O'boyle, A. L. Tenderholt and K. M. Langner, *J. Comput. Chem.*, 2008, **29**, 839–845.

19 K. Memminger, T. Oeser and T. J. J. Müller, *Org. Lett.*, 2008, **10**, 2797–2800.

20 C. R. Newman, C. D. Frisbie, D. A. da Silva Filho, J. L. Brédas, P. C. Ewbank and K. R. Mann, *Chem. Mater.*, 2004, **16**, 4436–4451.

21 (*a*) P. Thordarson, *Chem. Soc. Rev.*, 2011, **40**, 1305–1323; (*b*) *Non-linear least-squares curve fitting were carried out with the online software Bindfit*. **https://supramolecular.org**, (accessed 2022-4-10).

22 (*a*) J. Xie, X. Li, S. Wang, A. Li, L. Jiang and K. Zhu, *Nat. Commun.*, 2020, **11**, 3348; (*b*) T. A. Barendt, W. K. Myers, S. P. Cornes, M. A. Lebedeva, K. Porfyrakis, I. Marques, V. Félix and P. D. Beer, *J. Am. Chem. Soc.*, 2020, **142**, 349–364.

23 V. G. Jiménez, A. H. G. David, J. M. Cuerva, V. Blanco and A. G. Campaña, *Angew. Chem., Int. Ed.*, 2020, **59**, 15124–15128.

24 Anon, *The Carbonyl Group*, **https://chem.libretexts.org/@go/page/747**, (accessed 2022-5-10).

25 D. Flaig, M. Maurer, M. Hanni, K. Braunger, L. Kick, M. Thubauville and C. Ochsenfeld, *J. Chem. Theory Comput.*, 2014, **10**, 572–578.

26 (*a*) A. R. Mohebbi, J. Yuen, J. Fan, C. Munoz, M. f. Wang, R. S. Shirazi, J. Seifter and F. Wudl, *Adv. Mater.*, 2011, **23**, 4644–4648; (*b*) K. Kawabata, M. Saito, I. Osaka and K. Takimiya, *J. Am. Chem. Soc.*, 2016, **138**, 7725–7732.